# Switching Orientation of Two Axial Imidazole Ligands between Parallel and Perpendicular in Low-Spin Fe(III) and Fe(II) Nonplanar Porphyrinates

**ARTICLE** *in* INORGANIC CHEMISTRY · OCTOBER 2012

Impact Factor: 4.76 · DOI: 10.1021/ic300229u · Source: PubMed



**5 AUTHORS**, INCLUDING:

Ranjan Patra
Atomic Energy and Alternative Energies Com…
**22** PUBLICATIONS **313** CITATIONS
SEE PROFILE

Soumyajit Dey
Temple University
**8** PUBLICATIONS **42** CITATIONS
SEE PROFILE

Debangsu Sil
Indian Institute of Technology Kanpur
**8** PUBLICATIONS **36** CITATIONS
SEE PROFILE

Inorganic Chemistry

Article

pubs.acs.org/IC

# Switching Orientation of Two Axial Imidazole Ligands between Parallel and Perpendicular in Low-Spin Fe(III) and Fe(II) Nonplanar Porphyrinates

Ranjan Patra, Dipankar Sahoo, Soumyajit Dey, Debangsu Sil, and Sankar Prasad Rath*

Department of Chemistry, Indian Institute of Technology Kanpur, Kanpur-208016, India

Supporting Information

**ABSTRACT:** We have reported here the synthesis, structure, and properties of low-spin bis-imidazole-coordinated Fe(III) and Fe(II) complexes of 5,10,15,20-tetrakis-(pentafluorophenyl)-2,3,7,8,12,13,17,18-octachloroporphyrin, $[Fe^{III}(TFPPCl_8)(L)_2]ClO_4$ and $Fe^{II}(TFPPCl_8)(L)_2$ (L = 1-methylimidazole, 4-methylimidazole, imidazole). The X-ray structure of $Fe^{II}(TFPPCl_8)(1\text{-MeIm})_2$ is reported here, which demonstrated the near-perpendicular axial ligand orientation (dihedral angle between two 1-methylimidazoles is 80.7°) for Fe(II) porphyrins in a highly saddle-distorted macrocyclic environment. Oxidation of $Fe^{II}(TFPPCl_8)(L)_2$ using thianthrenium perchlorate produces $[Fe^{III}(TFPPCl_8)(L)_2]ClO_4$, which was also isolated in the solid state and characterized spectroscopically. The complex gives rhombic EPR spectra in both solid and solution phases at 77 K and thus represents a rare example of nearly parallel axial ligand orientations for the unhindered imidazoles in a saddle-distorted porphyrin macrocycle. Geometry optimization using DFT also converged to the parallel axial alignment when 1-methylimidazole was used as the axial ligand (the dihedral angle between two axial ligands is 8.6°). The potential energy surface (PES) scan results also show that the relatively parallel axial orientations are energetically preferred for Fe(III), while perpendicular orientations are preferred for the Fe(II) complexes reported here. Bulk oxidation of $Fe^{II}(TFPPCl_8)(L)_2$ in dichloromethane at a constant potential under nitrogen converts it to $[Fe^{III}(TFPPCl_8)(L)_2]ClO_4$, which gives identical EPR spectra at 77 K and which upon reduction regenerates $Fe^{II}(TFPPCl_8)(L)_2$ again. Thus, we have demonstrated here very rare examples of Fe porphyrins in which the relative axial imidazole orientations switch between parallel and perpendicular just upon changing the oxidation states of iron from +3 to +2, respectively, in a nonplanar porphyrinic environment. These observations could be immensely important for understanding the possible effects of axial histidine orientations on similar macrocyclic deformations observed in various heme proteins.

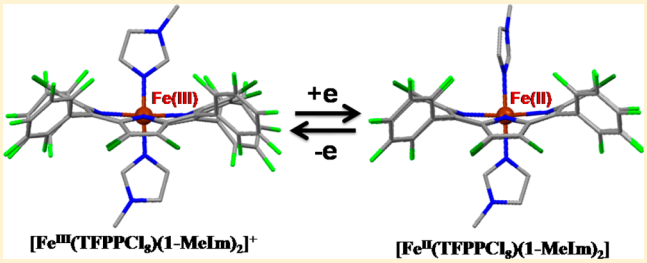


## INTRODUCTION

Heme-containing electron-transfer proteins are essential to many biological processes. Bis-histidine coordinated heme centers are well-known to be involved in electron transfer in a number of cytochrome-containing systems which shuttle between iron(II) and iron(III) oxidation states. In addition to relatively small molecular weight heme proteins,[1,2] a number of cytochrome-containing multiheme proteins with bis-histidine coordination are also known[3−7] which include the cytochrome *b* of mitochondrial complexes II,[4] III,[5] and chloroplasts,[6] cytochrome *a* of mitochondrial complex IV,[7e] and a number of multiheme cytochromes *c*.[7a−d,f] Crystallographic investigation of hemoproteins with two imidazole (histidine) axial ligands showed that a number of hemoproteins have relative parallel oriented ligands which include cytochromes $b_5$,[1b] three of the heme centers of cytochromes $c_3$,[8a−d] flavocytochrome $b_2$,[8e] and the heme *a* of cytochrome oxidase.[8f] In contrast, structural characterizations of several other hemoproteins such as *b* hemes of cytochrome $b_6f$ of chloroplasts[6c,d] and one of the *c*-type hemes of cytochrome $c_3$[8a−d] have been found to have a relative perpendicular arrangement of two imidazole ligands. On the basis of EPR and NMR spectroscopic data of the oxidized (Fe(III)) forms, two axial imidazole planes of many heme proteins can also be identified oriented either parallel (such as the *b* hemes of sulfite oxidase[9a]) or perpendicular (such as *b* hemes of mitochondrial complex III, also known as cytochrome $bc_1$,[9b−d] and the *c*-type heme of cytochrome *c*″ of *Methylophilus methylotrophus*[9e−g]). It is believed that the arrangement of the axial ligands plays an important role in defining the spectroscopic properties and also the reduction potentials of these heme centers. For example, at the highest resolution obtained thus far (2.1 Å),[10a] the bovine cytochrome $bc_1$ complex structure has the two *b* heme centers having axial histidine (imidazole) plane dihedral angles of 64 and 86°; the yeast structure, with highest resolution 2.3 Å,[5b,d] has those angles as 71 and 84°. The reduction potentials of former ($b_H$) and latter ($b_L$) heme centers of murine Complex III are +92 ± 14 and −31 ± 12 mV,[10b] respectively, and for other mammalian *b* heme centers, the values are similar. Depending on the

**Received:** January 31, 2012
**Published:** October 22, 2012

character of the electronic ground state, the complexes with parallel and perpendicular orientations of the axial ligands have different spectroscopic properties. Model systems have been great aids in correlating the structure of heme centers with their spectroscopic properties.

The heme cofactor is an aromatic, highly conjugated macrocycle that adopts a planar conformation when free in solution. However, evidence from high-resolution crystal structures and spectroscopic studies has shown that the heme macrocycle displays a range of distorted nonplanar shapes, which are presumably caused by proteins.[11−17] Importantly, modes of porphyrin distortion, while energetically unfavorable,[15] are conserved within hemoproteins, suggesting that such distortions are likely to be important for protein function. We have presented earlier a family of five- and six-coordinated high-spin Fe(III) porphyrins in a distorted macrocyclic environment which enable us to scrutinize the effects of axial ligand coordination and macrocycle deformations on metal ion displacement, as a part of our ongoing research on nonplanar heme.[18,19] It has also been suggested that the displacements of iron in proteins are the consequences of nonequivalent axial coordination as well as protein-induced deformation at heme.[19a] It would be thus interesting to investigate the axial ligand orientations on the nonplanar porphyrinic environment in order to understand the effects of similar distortions observed in various heme proteins. It is expected that the axial ligands and their relative orientation can alter the electronic and magnetic properties as well as the reduction potentials in various heme proteins.

The influence of interaction of axially coordinated ligands with an Fe−porphyrin core (planar porphyrin without substituent) has been studied by quantum chemical calculations. Density functional theory (DFT) calculations on $Fe(por)(Im)_2$ and $Fe(por)(Im)_2^+$ (por = porphyrin, Im = imidazole) showed that there is no difference in the preference for parallel or orthogonal orientations of imidazoles for both Fe(II) and Fe(III) complexes, since they almost have identical energies,[20] which is also in agreement with the experimental data.[21,22] However, experimental and theoretical studies on heme model systems have shown that the orientations of axial ligands have an influence on porphyrin ring conformations. In complexes with a parallel orientation of two planar axial ligands, the porphyrin ring remains planar. On the other hand,in porphyrin complexes that have two planar axial ligands in a perpendicular orientation, the porphyrin ring is almost invariably distorted from planarity.[23,24] Previous studies indicate that the orientation (and hence rotation) of axial ligands may be closely related to how much the porphyrin ring can be distorted from planarity.[21a,c,25] This suggests that studying the orientation and rotation of axial ligands in model hemes can provide information about the shape of the metalloporphyrin core, which eventually can be correlated to how much the porphyrin ring may be distorted from planarity in analogous heme proteins.

Previously, it was demonstrated by us that the parallel axial orientations are preferred for unhindered imidazoles in a distorted Fe(III) tetranitrooctaethylporphyrin, while perpendicular axial orientations are preferred for the corresponding Fe(II) complex.[18] It was still unclear what factors have a dominant influence on such preferential orientation of axial ligands. Since it was demonstrated that substituents on the porphyrin ring (propionic groups) have an influence on the orientation of imidazoles in heme proteins,[16b,c] one can assume a similar influence of substituents in iron−porphyrinato complexes. This has prompted us to investigate further, whether or not the orientation preference of axial ligand on oxidation states of iron is also observed for the nonplanar TPP-type (TPP = tetraphenylporphyrin) porphyrinic systems as well. An ideal model system would allow the metal oxidation states to be varied without altering the native heme. Therefore, a series of bis-imidazole-coordinated Fe(II) and Fe(III) porphyrins containing highly nonplanar TPP-type ligands have been synthesized and their axial ligand orientations have been scrutinized.

The macrocycles can be distorted by introducing sterically demanding substituents in the porphyrin periphery. This objective has been achieved successfully by taking the 5,10,15,20-tetrakis(pentafluorophenyl)-2,3,7,8,12,13,17,18-octachloroporphyrin ($H_2TFPPCl_8$) macrocycle, in which the presence of eight electron-withdrawing bulky chloro groups at the $\beta$-positions severely distorts the porphyrin geometry. We have reported here the parallel and perpendicular orientation preferences of two unhindered imidazoles as axial ligands while coordinated to Fe(III) and Fe(II) porphyrins, respectively, in a nonplanar porphyrinic environment.

## RESULTS AND DISCUSSION

The free ligand 5,10,15,20-tetrakis(pentafluorophenyl)-2,3,7,8,12,13,17,18-octachloroporphyrin ($H_2TFPPCl_8$) was synthesized by using the literature method.[26] Iron was then inserted into the macrocycle by refluxing the free ligand in DMF with $FeCl_2$ under nitrogen for nearly 2.5 h followed by chromatographic separation in silica gel using chloroform as eluent, which produce $Fe^{III}(TFPPCl_8)Cl$ (**1**) in excellent yields. The UV−vis spectrum of the complex shows one broad Soret band at 430 nm and a Q band at 594 nm. The Soret band of the compound **1** is red-shifted by 14 and 12 nm compared to those of $Fe^{III}(TPP)Cl$ and $Fe^{III}(TFPP)Cl$, respectively.[27] The bathochromic shift and broadening of the Soret band, as observed in **1**, are due to macrocyclic distortion. The EPR spectral measurements carried out at 77 K of the sample show similar spectral features in both the solid and solution phase. The spectra are axially symmetric with $g_\perp = 5.96$ and $g_\parallel = 2.01$ for the frozen toluene solution and $g_\perp = 5.98$ and $g_\parallel = 2.01$ for the powder. These results provide unequivocal evidence for the high-spin nature of the complex in both solid and solution phases.

Addition of axial ligand L (L= 1-methylimidazole, 4-methylimidazole, imidazole) to the benzene solution of **1** results in spontaneous autoreduction to produce air-stable $Fe^{II}(TFPPCl_8)(L)_2$ in quantitative yield; Figure 1 shows time evaluation spectral changes of **1** in the presence of excess 1-methylimidazole, in which peaks at 430 and 594 nm correspond to $Fe^{III}(TFPPCl_8)Cl$ (**1**) transformed to peaks at 350, 446, 552, and 582 nm that are characteristic of $Fe^{II}(TFPPCl_8)(1\text{-MeIm})_2$ (**2**). Similar results are also obtained with other imidazoles as axial ligands.

The autoreduction of iron(III) porphyrins has long been known,[28] and generally, two types of mechanisms have been reported for such autoreduction. One is base-catalyzed autoreduction using piperidine, alkoxide, cyanides, etc. in which the reduction of iron is accompanied by one-electron oxidation of the substrates.[28d,e] The electron-transfer step is facilitated by the deprotonation of coordinated base by free base. In another mechanism, the iron atom ligated to an electron-deficient macrocycle has strong Lewis acidity that


dx.doi.org/10.1021/ic300229u | Inorg. Chem. 2012, 51, 11294−11305

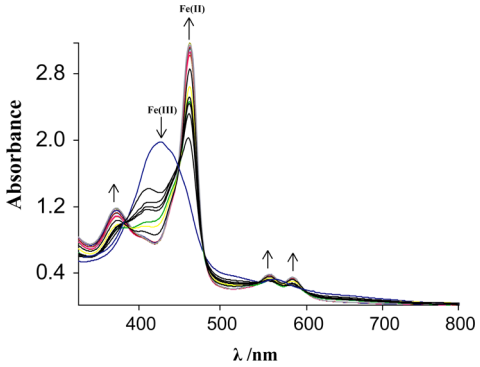


**Figure 1.** Time-evolution spectral changes (at 298 K) of $Fe^{III}(TFPPCl_8)Cl$ in benzene (~$10^{-6}$ M) in the presence of excess 1-methylimidazole, which produces $Fe^{II}(TFPPCl_8)(1\text{-MeIm})_2$ (**2**). The arrows indicate an increase or decrease of band intensity with time. Spectra were recorded over the span of 30 min. Isosbestic points (nm): 363, 431, 465, 536, and 597.

results in autoreduction to Fe(II) porphyrin in the presence of an axial ligand such as pyridine and imidazoles.[28a,c] For example, ferric complexes of dioxoporphodimethene and tetranitrooctaethylporphyrin, in the presence of pyridine, autoreduce spontaneously to diamagnetic bis(pyridine)iron(II) complexes, while the corresponding Fe(III) octaethylporphyrins do not.[19e,28c] The ease of reduction is likely a result of the increased Lewis acidity of the iron center due to the large number of electronegative substituents on the porphyrin macrocycles. Scheme 1 shows the synthetic outline of the complexes reported here and their abbreviations.

**Crystallographic Characterization of $Fe^{II}(TFPPCl_8)(1\text{-MeIm})_2$ (2).** Dark red crystals of **2** were grown by slow diffusion of *n*-hexanes into tetrahydrofuran solutions of $Fe^{III}(TFPPCl_8)Cl$ containing 1-methylimidazole (1/10) at room temperature in air. The complex crystallizes in the tetragonal crystal system with $I4_1/a$ space group. Perspective views of the molecule are shown in Figure 2. Selected bond

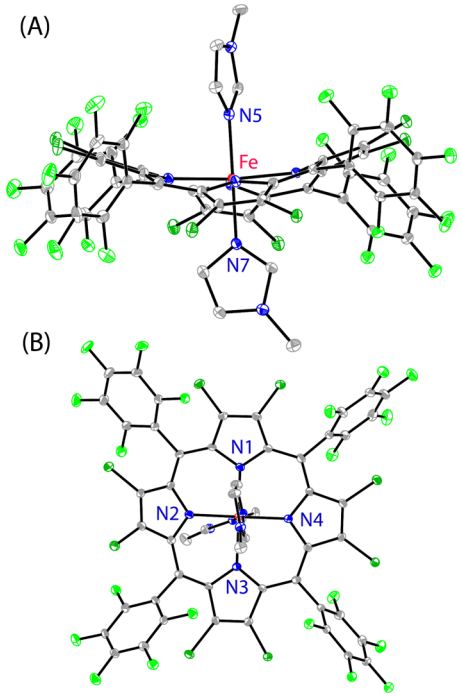


**Figure 2.** Two perspective views (A, side view; B, top view) of $Fe^{II}(TFPPCl_8)(1\text{-MeIm})_2$ (**2**) showing 50% thermal contours for all non-hydrogen atoms at 100 K. Hydrogen atoms have been omitted for clarity.

**Scheme 1**

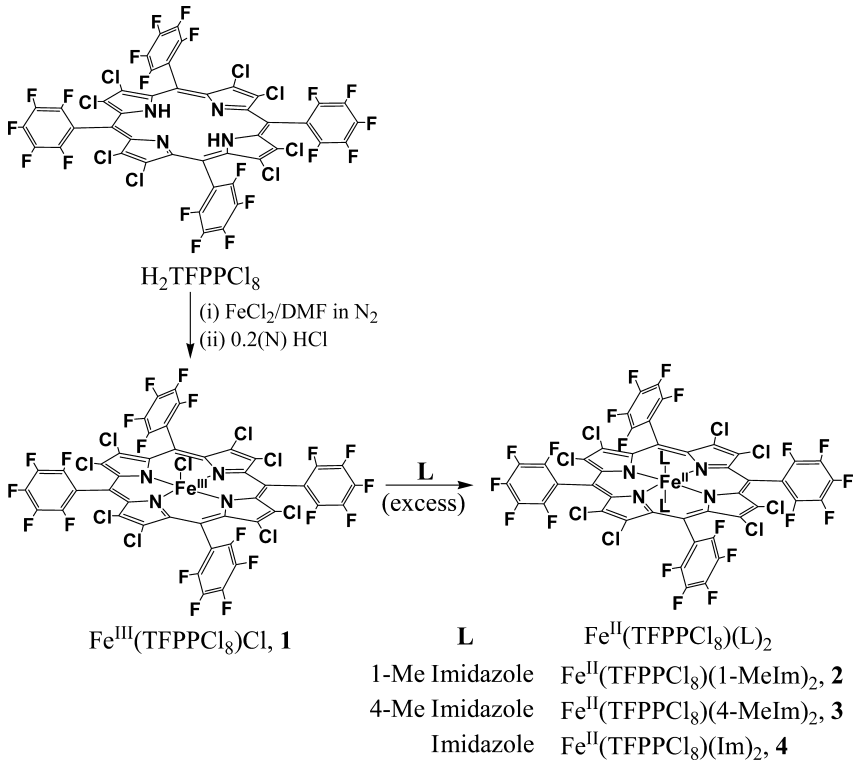



dx.doi.org/10.1021/ic300229u | *Inorg. Chem.* 2012, 51, 11294–11305

distances and angles are shown in Table 1, while crystal data and data collection parameters are given in Table 2. As seen

**Table 1. Selected Bond Lengths (Å) and Angles (deg) for $Fe^{II}(TFPPCl_8)(1\text{-MeIm})_2$ (2)**

| | | | |
|---|---|---|---|
| Fe−N1 | 1.984(5) | Fe−N4 | 1.968(5) |
| Fe−N2 | 1.996(5) | Fe−N5 | 1.999(5) |
| Fe−N3 | 1.976(5) | Fe−N7 | 1.997(5) |
| N1−Fe−N2 | 90.4(2) | N3−Fe−N5 | 92.5(2) |
| N1−Fe−N3 | 173.9(2) | N4−Fe−N5 | 89.1(2) |
| N1−Fe−N4 | 90.24(19) | N1−Fe−N7 | 86.38(19) |
| N2−Fe−N3 | 89.91(19) | N2−Fe−N7 | 93.3(2) |
| N2−Fe−N4 | 173.3(2) | N3−Fe−N7 | 87.55(19) |
| N3−Fe−N4 | 90.19(19) | N4−Fe−N7 | 93.4(2) |
| N1−Fe−N5 | 93.6(2) | N5−Fe−N7 | 177.5(2) |
| N2−Fe−N5 | 84.2(2) | | |

**Table 2. Crystal Data and Data Collection Parameters of $Fe^{II}(TFPPCl_8)(1\text{-MeIm})_2$ (2)**

| | |
|---|---|
| formula | $C_{52}H_{12}Cl_8F_{20}FeN_8$ |
| *T*, K | 100(2) |
| formula wt | 1468.15 |
| cryst syst | tetragonal |
| space group | $I4_1/a$ |
| *a*, Å | 28.611(4) |
| *b*, Å | 28.611(4) |
| *c*, Å | 25.302(6) |
| *α*, deg | 90 |
| *β*, deg | 90 |
| *γ*, deg | 90 |
| *V*, Å$^3$ | 20 713(6) |
| radiation (*λ*, Å) | Mo K*α* (0.710 73) |
| *Z* | 16 |
| $d_{calcd}$, g.cm$^{-3}$ | 1.883 |
| *F*(000) | 11552 |
| cryst size (mm$^3$) | 0.18 × 0.14 × 0.10 |
| *μ*, mm$^{-1}$ | 0.827 |
| no. of unique data | 11300 |
| no. of restraints | 0 |
| no. of params refined | 804 |
| GOF on $F^2$ | 1.011 |
| R1[a] ($I>2\sigma(I)$) | 0.0692 |
| R1[a] (all data) | 0.1386 |
| wR2[b] (all data) | 0.1841 |

[a] $R1 = (\sum||F_o| - |F_c||)/\sum|F_o|$. [b] $wR2 = ((\sum[w(F_o^2 - F_c^2)^2])/(\sum[w(F_o^2)^2])^{1/2}$.

from Table 1, Fe−$N_p$ distances are in the narrow range of 1.968−1.996 Å, while the two Fe−$N_{ax}$ distances are 1.999(5) and 1.997(5) Å. These distances fall within the spread of literature values observed for low-spin iron(II) porphyrinates containing two imidazoles as axial ligands.[18,19,27,29] Two 1-methylimidazole axial ligands in **2** make an 80.7° angle with each other and also form 20.9 and 14.8° dihedral angles between the plane of the closest $N_p$−Fe−$N_{ax}$ and the axial ligand plane. The X-ray structure clearly demonstrates nearly perpendicular axial ligand orientations with unhindered 1-methylimidazole as an axial ligand in a distorted macrocyclic environment. A diagram illustrating the molecular packing in the unit cell is shown in Figure S1 (see the Supporting Information), which does not show any unusual interactions between the molecules in the crystal lattice. The porphyrin ring is highly distorted in the complex and is best appreciated by turning to Figure 3, where the out-of-plane displacements in

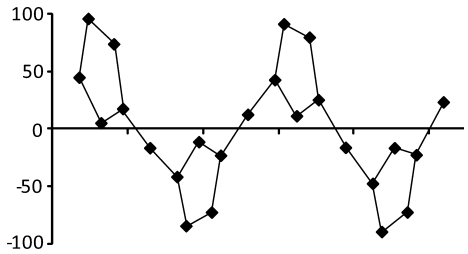


**Figure 3.** Out-of-plane displacements (in units of 0.01 Å) of the porphyrin core atoms of $Fe^{II}(TFPPCl_8)(1\text{-MeIm})_2$ (**2**) from the least-squares plane of the $C_{20}N_4$ porphyrinato core.

units of 0.01 Å of the porphyrin core atoms are compared. As can be seen, the ring distortions of the complex can be described as saddle-type with alternating displacement of the pyrrole rings below and above the mean porphyrin plane, while the pyrrole nitrogen and meso carbons are placed near the plane.

Table 3 describes selected structural parameters of Fe(II) porphyrins reported here and elsewhere that contain imidazole/substituted imidazole as an axial ligand. It was found that, for low-spin Fe(II) centers,[18,29] parallel orientations of axial imidazole ligands are exclusively observed when planar porphyrins are used. As can be seen, complexes such as $Fe^{II}(TPP)(1\text{-VinIm})_2$, $Fe^{II}(TPP)(1\text{-BzylIm})_2$, and $Fe^{II}(TPP)(1\text{-MeIm})_2$ have a nearly planar porphyrin core as well as unhindered imidazoles as axial ligand and thus stabilize a nearly parallel orientation of axial ligands. Complexes such as $Fe^{II}(TpivPP)(1\text{-MeIm})_2$, $Fe^{II}(TpivPP)(1\text{-EtIm})_2$, and $Fe^{II}(TpivPP)(1\text{-VinIm})_2$ have a nearly perpendicular axial orientation, even though they all have a nearly planar porphyrin core and unhindered axial imidazole ligands (TpivPP = *R,R,R,R*-tetrakis(*o*-pivalamidophenyl)porphyrin).[29a] Here, the "picket fence" environment provides strong steric interactions that force the axial ligands to arrange in perpendicular orientations. For $Fe^{II}(TMP)(2\text{-MeIm})_2$, however, a near-perpendicular ligand orientation results due to bulky 2-methylimidazole as axial ligand (TMP = tetramesitylporphyrin).[29c] In sharp contrast, $Fe^{II}(TFPPCl_8)(1\text{-MeIm})_2$ demonstrates a near-perpendicular axial ligand orientation even with unhindered imidazoles but in a highly nonplanar TPP-type macrocyclic environment. As can be seen in Table 3, the porphyrin ring distorted most ($\Delta_{24}$) in $Fe^{II}(TFPPCl_8)(1\text{-MeIm})_2$ (**2**) while the dihedral angles between the planes of the closest $N_p$−Fe−$N_{ax}$ and the axial imidazole are also lowest in $Fe^{II}(TFPPCl_8)(1\text{-MeIm})_2$, except for "picket fence" porphyrinates, where the axial ligands are forced to have certain arrangements. Earlier, we have also observed nearly perpendicular axial ligand orientations in $Fe^{II}(tn\text{-OEP})(1\text{-MeIm})_2$ where a distorted OEP-type macrocycle has been used (*tn*-OEP = 5,10,15,20-tetranitrooctaethylporphyrin).[18] It would be interesting to compare with low-spin bis-pyridine-coordinated Fe(II) porphyrins. For the structurally characterized bis-pyridine complexes reported so far, parallel orientations of two unhindered pyridines are exclusively observed for planar porphyrin while perpendicular orientations are observed for nonplanar porphyrins.[19e,27,30] For example, two axial pyridine ligands are perpendicularly oriented in $Fe^{II}(tn\text{-OEP})(L)_2$ (L =


dx.doi.org/10.1021/ic300229u | Inorg. Chem. 2012, 51, 11294−11305

**Table 3. Selected Geometrical Parameters for $Fe^{II}(por)(L)_2$ (L = Imidazoles)[a]**

| compd | $Fe-N_p$[b] | $Fe-N_{ax}$ | $\Phi$[c] | $\theta$[d] | $\Delta_{24}$[e] | ref |
|---|---|---|---|---|---|---|
| $Fe^{II}(TFPPCl_8)(1\text{-MeIm})_2$ | 1.981(5) | 1.999(5) | 20.9 | 80.7 | 0.48 | this work |
| | | 1.997(5) | 14.8 | | | |
| $Fe^{II}(tn\text{-OEP})(1\text{-MeIm})_2$ | 1.982(2) | 2.000(2) | 32.2 | 80.9 | 0.46 | 18 |
| | | 2.007(2) | 23.8 | | | |
| $Fe^{II}(tn\text{-OEP})(1\text{-MeIm})_2$.THF | 1.985(3) | 1.999(3) | 30.0 | 89.8 | 0.44 | 18 |
| | | 2.002(3) | 30.3 | | | |
| $Fe^{II}(TMP)(2\text{-MeIm})_2$ mol-1 | 1.964(5) | 2.030(3) | 41.1 | 82.4 | 0.25 | 29c |
| | | 2.047(3) | 41.4 | | | |
| $Fe^{II}(TMP)(2\text{-MeIm})_2$ mol-2 | 1.961(7) | 2.032(3) | 44.8 | 84.4 | 0.25 | 29c |
| | | 2.028(3) | 37.9 | | | |
| $Fe^{II}(TPP)(4\text{-MeIm})_2$ | 1.9952(8) | 2.0154(8) | 0.7 | 0 | nearly planar | 29b |
| $Fe^{II}(TPP)(1\text{-VinIm})_2$ | 2.001(2) | 2.004(2) | 14 | 0 | nearly planar | 29d |
| $Fe^{II}(TPP)(1\text{-BzylIm})_2$ | 1.993(9) | 2.017(4) | 26 | 0 | nearly planar | 29d |
| $Fe^{II}(TPP)(1\text{-MeIm})_2$ | 1.997(6) | 2.014(5) | 15 | 0 | nearly planar | 29c |
| $Fe^{II}(TpivPP)(1\text{-MeIm})_2$ | 1.992(3) | 1.9958(19) | 8.5 | 77.2 | nearly planar | 29a |
| | | 1.9921(18) | 21.1 | | | |
| $Fe^{II}(TpivPP)(1\text{-EtIm})_2$ | 1.993(6) | 2.0244(18) | 6.6 | 62.4 | nearly planar | 29a |
| | | 1.9940(19) | 20.7 | | | |
| $Fe^{II}(TpivPP)(1\text{-VinIm})_2$ | 1.988(5) | 1.9979(19) | 11.2 | 78.5 | nearly planar | 29a |
| | | 1.9866(18) | 24.5 | | | |

[a]Abbreviations: 1-VinIm, 1-vinylimidazole; 1-BzylIm, 1-benzylimidazole; 1-MeIm, 1-methylimidazole; 2-MeIm, 2-methylimidazole; 4-MeIm, 4-methylimidazole; 5-MeIm, 5-methylimidazole; 1,2-$Me_2$Im, 1,2-dimethylimidazole [b]Average value in Å. [c]Dihedral angle (deg) between the plane of the closest $N_p-Fe-N_{ax}$ and the axial ligand plane. [d]Dihedral angle (deg) between two axial ligands. [e]Average displacement of atoms in Å from the least-squares plane of the $C_{20}N_4$ pophyrinato core.

**Scheme 2**

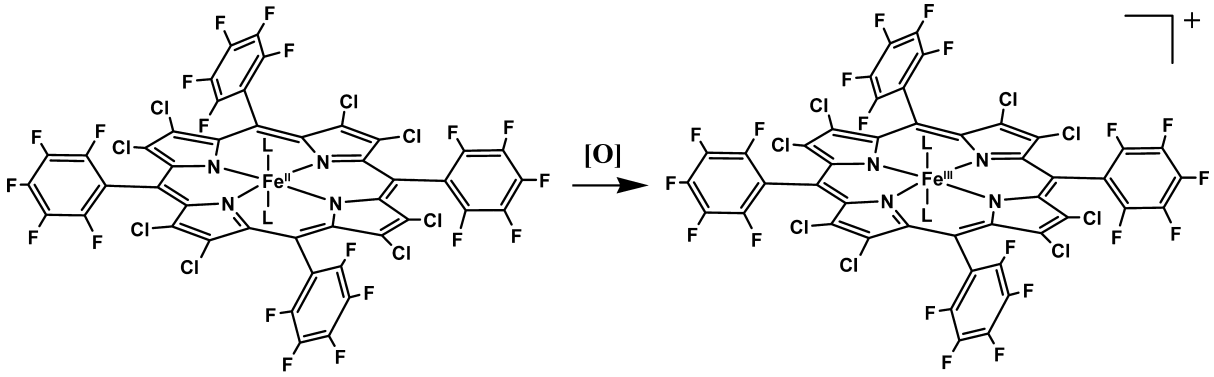


$Fe^{II}(TFPPCl_8)(L)_2$ $[Fe^{III}(TFPPCl_8)(L)_2]ClO_4$

$[Fe^{III}(TFPPCl_8)(1\text{-MeIm})_2]ClO_4$, **5**

$[Fe^{III}(TFPPCl_8)(4\text{-MeIm})_2]ClO_4$, **6**

$[Fe^{III}(TFPPCl_8)(Im)_2]ClO_4$, **7**

pyridine, 3-chloropyridine, 4-cyanopyridine),[19e] $Fe^{II}\{(COOMe)_8TPBP\}(py)_2$,[30b] and $Fe^{II}(TFPPBr_8)(py)_2$,[27d] in which the porphyrins are highly nonplanar ($TFPPBr_8$ = 2,3,7,8,12,13,17,18-octabromo-5,10,15,20-tetrakis-(pentafluorophenyl)porphyrin, py = pyridine). These results clearly demonstrated that the perpendicular orientation of unhindered axial ligands in Fe(II) porphyrin is due to the highly nonplanar geometry of the porphyrin, irrespective of its nature.

To investigate the axial ligand orientation for Fe(III) porphyrins in detail, imidazole ligated six-coordinated $[Fe^{III}(TFPPCl_8)(L)_2]^+$ has been synthesized by the oxidation of the corresponding $Fe^{II}(TFPPCl_8)(L)_2$ complex using thianthrenium perchlorate as an oxidizing agent. Scheme 2 represents the synthetic outline of bis-imidazole-coordinated Fe(III) porphyrins reported here along with their abbreviations. In spite of several attempts, we were unable to get X-ray-quality crystals of $[Fe^{III}(TFPPCl_8)(L)_2]ClO_4$ suitable for structure determination but the electronic and molecular structures have been determined using various spectroscopic techniques and DFT investigations.

The EPR spectral measurements have been carried out for $[Fe^{III}(TFPPCl_8)(L)_2]ClO_4$ at 77 K which show similar rhombic type spectral features both in solid and solution; Figure 4 shows the X-band EPR spectra in dichloromethane. The spectra were then carefully simulated (a representative simulated spectrum is shown in Figure S2; see the Supporting Information), which provided the following $g$ values: $g_3$ = 2.87, $g_2$ = 2.28, and $g_1$ =


dx.doi.org/10.1021/ic300229u | Inorg. Chem. 2012, 51, 11294−11305

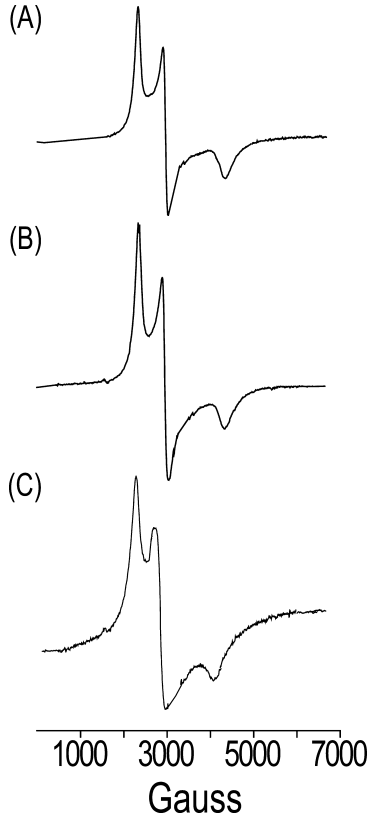


**Figure 4.** X-band EPR spectra of (A) $[Fe^{III}(TFPPCl_8)(1\text{-}MeIm)_2]ClO_4$ (**5**), (B) $[Fe^{III}(TFPPCl_8)(4\text{-}MeIm)_2]ClO_4$ (**6**), and (C) $[Fe^{III}(TFPPCl_8)(Im)_2]ClO_4$ (**7**) in dichloromethane at 77 K.

1.56 ($\sum g^2$=15.87) for **5**; $g_3$ = 2.85, $g_2$ = 2.28, and $g_1$ = 1.59 ($\sum g^2$ = 15.85) for **6**; $g_3$ = 2.88, $g_2$ = 2.30, and $g_1$ = 1.57 ($\sum g^2$ = 16.04) for **7**. Such a smaller spread of $g$ values has also been observed in various low-spin ferrihemes in $CH_2Cl_2/CHCl_3$ such as $[Fe^{III}(OMTPP)(Im)_2]ClO_4$ ($g_3$ = 2.84, $g_2$ = 2.31, and $g_1$ = 1.58),[31a] $[Fe^{III}(OETPP)(Im)_2]ClO_4$ ($g_3$ = 2.72, $g_2$ = 2.37, and $g_1$ = 1.64),[31a] $[Fe^{III}(tn\text{-}OEP)(1\text{-}MeIm)_2]ClO_4$ ($g_3$ = 2.79, $g_2$ = 2.32, and $g_1$ = 1.69),[18] $[Fe^{III}(TMP(1\text{-}MeIm)_2]ClO_4$ ($g_3$ = 2.89, $g_2$ = 2.33, and $g_1$ = 1.57),[31b] and $[Fe^{III}(TPP(1\text{-}MeIm)_2]Cl$ ($g_3$ = 2.876, $g_2$ = 2.289, and $g_1$ = 1.553),[31c] in which the electronic natures of the peripheral substituent vary widely (OMTPP = octamethyltetraphenylporphyrin, OETPP = octaethyltetraphenylporphyrin). Such types of spectra are typical for low-spin ($S$ = $^1/_2$) iron(III) porphyrins with a $(d_{xy})^2(d_{xz},d_{yz})^3$ electronic configuration. For ferriheme complexes with a $(d_{xy})^2(d_{xz},d_{yz})^3$ electronic ground state, rhombic EPR spectra have been associated with a mutually parallel orientation of the axial ligand planes and the "large $g_{max}$" type EPR spectra with a mutually perpendicular ligand plane.[13] For example, similar rhombic EPR spectra have also been observed for $[Fe^{III}(OMTPP)(1\text{-}MeIm)_2]Cl$, which has a saddle-distorted porphyrin core with 1-methylimidazole as the axial ligand; the X-ray structure of the molecule shows a nearly parallel axial ligand orientation (dihedral angle of 19.5°).[32a]

It has been shown earlier that, for the structurally characterized low-spin Fe(III) porphyrins for which the EPR spectra have been recorded, a plot of the largest $g$ value (independent of whether it is a "large $g_{max}$" or "normal rhombic" signal) vs the imidazole dihedral angle provides a fairly linear correlation with no break between complexes with these two types of EPR signals.[32b,c,33] The signal type of model hemes appears to change from the "large $g_{max}$" to "normal rhombic" at ~57° with continuous changes in the largest $g$ value upon changing the dihedral angle between the axial ligand planes from 90° to 0°.[32b,c] Judging by the size of the largest $g$ values obtained for all three saddle-distorted complexes reported here, dihedral angles close to 10° are obtained from the average correlation line of model hemes ,which are also in close agreement with the value obtained from geometry optimization of the complex by DFT (vide infra).

The d-orbital splitting pattern observed for low-spin $d^5$ systems is qualitatively presented in Scheme 3. The crystal

**Scheme 3**

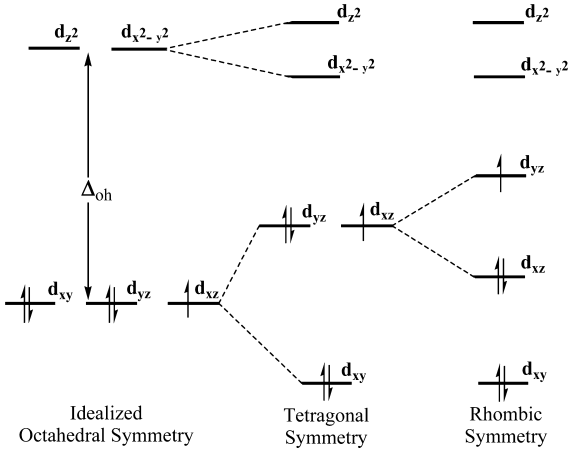


field splitting between the three lowest energy and the two highest energy d orbitals is in reality much larger in all cases than the splitting within the lower and higher energy subsets. For these ferriheme systems, the porphyrin ring is of somewhat lower crystal field than that of the axial imidazole ligands, which leads to a tetragonal distortion of the complex.[16a] Perpendicularly oriented planar axial ligands give rise to this tetragonal splitting pattern, in which the $d_{xz}$, $d_{yz}$ set (also called the $d_\pi$ set) is degenerate. With five electrons in the three low-lying d orbitals ($d_{xy}$, $d_{xz}$, and $d_{yz}$), there is an odd electron in the $d_\pi$ set that results in an unstable situation for the complex because of the Jahn–Teller effect.[16a] However, if the planar axial ligands are in parallel planes, a rhombic distortion is introduced, where the degeneracy of the $d_{xz}$ and $d_{yz}$ orbitals is lifted.[16a] The rhombic splitting pattern is thus lower in overall energy than the tetragonal or octahedral splitting patterns, which leads to stabilization of the parallel orientation of the axial ligand. In heme proteins, however, axial ligands can be placed in a particular orientation by the design of the protein.

However, the "large $g_{max}$" EPR signal was shown to occur for ferriheme complexes with a $(d_{xy})^2(d_{xz},d_{yz})^3$ electronic ground state in which the splitting between the $d_{xz}$ and $d_{yz}$ orbitals is small (usually less than the value of the spin–orbit coupling constant, $\lambda$).[13] The structures of $[Fe^{III}(OETPP)(1\text{-}MeIm)_2]Cl$ and $[Fe^{III}(OMTPP)(1\text{-}MeIm)_2]Cl$, crystallized from chloroform-$d$/cyclohexane, were characterized by dihedral angles of 73.1 and 90°, respectively, between two axial imidazole planes. The porphyrin cores were found mostly saddle-distorted, while the crystals exhibited "large $g_{max}$" type EPR signals with $g_{max}$ = 3.27 and 3.61, respectively.[32a] The EPR spectra of frozen solutions of $[Fe^{III}(OMTPP)(4\text{-}Me_2NPy)_2]Cl$ and $[Fe^{III}(OMTPP)(2\text{-}MeIm)_2]Cl$ in $CD_2Cl_2$ also have "large $g_{max}$" type signals with $g_{max}$ = 3.29 and 3.27, respectively,


dx.doi.org/10.1021/ic300229u | Inorg. Chem. 2012, 51, 11294–11305

while the porphyrin cores are mostly saddle-distorted (4-$Me_2$NPy = 4-*N*,*N*-dimethylpyridine).[32e]

The orientations of planar axial ligands in bis-imidazole-ligated iron(III) porphyrins have been investigated for quite some time.[32] It was observed that a highly nonplanar porphyrin geometry is required to force the relative perpendicular orientation of planar axial ligands. Another set of strategies used for synthesizing complexes with relative perpendicular axial orientations is the use of sterically hindered imidazoles such as 2-methylimidazole. The presence of both parallel and perpendicular axial ligand orientations for the $[Fe^{III}(OEP)(2\text{-MeIm})_2]^+$ core are interesting. The elongation of the Fe−$N_p$ and Fe−$N_{ax}$ bond distances in $[Fe^{III}(OEP)(2\text{-MeIm})_2]ClO_4$ provides a means for alleviating steric contacts, and the nearly planar porphyrin core also leads to a parallel orientation of the axial ligands.[32h] On the other hand, short Fe−$N_p$ and Fe−$N_{ax}$ distances for $[Fe^{III}(OEP)(2\text{-MeIm})_2]Cl$ result in a highly nonplanar porphyrin core, which along with hindered 2-methylimidazole leads to nearly perpendicular axial orientations.[32d] Two crystalline forms with distinctly different axial ligand orientations, yet strikingly similar porphyrin core geometries, have been reported for $[Fe^{III}(OMTPP)(1\text{-MeIm})_2]Cl$. One form, *perp*-$[Fe^{III}(OMTPP)(1\text{-MeIm})_2]Cl$, has axial ligands in strictly perpendicular planes, while the second form, *paral*-$[Fe^{III}(OMTPP)(1\text{-MeIm})_2]Cl$, has the nearly parallel axial ligand orientation with a dihedral angle of 19.5°.[32a] Another interesting example was $[Fe^{III}(TMP)(5\text{-MeIm})_2]ClO_4$, which exists in two crystalline forms with distinctly different molecular structures. The structures differ in the relative orientation of the axial ligands. One form, *perp*-$[Fe^{III}(TMP)(5\text{-MeIm})_2]ClO_4$, has the axial ligands in a relative perpendicular orientation (the dihedral angle between the axial ligands is 76°), and the second form *paral*-$[Fe^{III}(TMP)(5\text{-MeIm})_2]ClO_4$ has the axial ligands in a relative parallel orientation (the dihedral angles between the axial ligands are 30 and 26° for the two different molecules in the unit cell). The porphyrin core in *perp*-$[Fe^{III}(TMP)(5\text{-MeIm})_2]ClO_4$ is found to be more distorted in comparison to that in *paral*-$[Fe^{III}(TMP)(5\text{-MeIm})_2]ClO_4$.[32g]

**Computational Studies.** Density functional calculations have been carried out for Fe(III) porphyrins, in which the atom coordinates are taken directly from the single-crystal X-ray data of the corresponding Fe(II) complex. Full geometry optimization has been obtained with 1-methylimidazole, as shown in Figure 5, using DFT, specifically the Becke three-parameter exchange functional (B3)[34] and the Lee−Yang−Parr correlation functional (LYP).[35] These B3LYP calculations have been carried out with the Gaussian 03, revision B.04, package.[36] The energy minimum occurs at the geometry where the two 1-methylimidazoles are oriented nearly parallel with an 8.6° dihedral angle (Figure 5), which is also in agreement with experiment (vide supra). The selected bond distances and angles for the optimized geometry are given in Table S1 (see the Supporting Information). The observation demonstrates the nearly parallel orientations of unhindered imidazoles in a highly saddle-distorted Fe(III) octachloropentafluorophenylporphyrin.

1D potential energy surface (PES) scans on both Fe(II) and Fe(III) six-coordinated complexes **2** and **5** have also been done by DFT; coordinates have been taken directly from the X-ray and optimized structures of the complexes, respectively. One axial ligand was then rotated in steps of 10°, keeping the other axial ligand intact in its position. The energy of the molecule

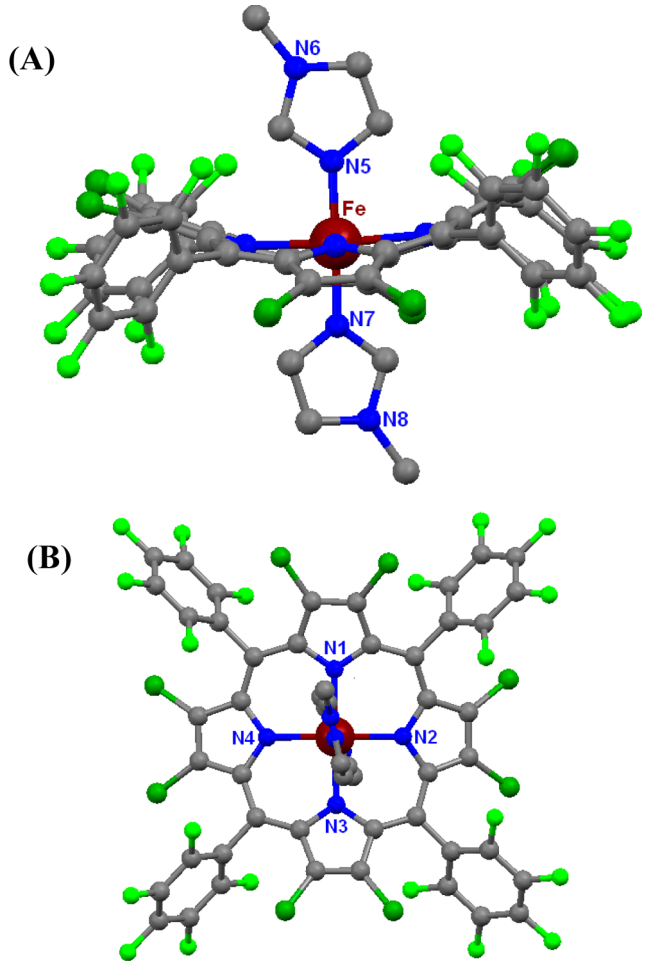


**Figure 5.** Two perspective views (A, side view; B, top view) of $[Fe^{III}(TFPPCl_8)(1\text{-MeIm})_2]^+$ obtained from full geometry optimization. Hydrogen atoms have been omitted for clarity.

was then plotted against the dihedral angle, as shown in Figure 6. For **5**, the lowest energy was observed when the dihedral angle between the axial ligands is ∼10°, and for **2**, the lowest energy was observed when the dihedral angle between the axial ligands is ∼80°, which is also in close agreement with the angle observed in the X-ray structure of the complex. For Fe(III) porphyrin with two axial 1-methylimidazoles, the energy minimum observed is nearly 10° because of the stabilization of the rhombic geometry. When the two axial ligands are in a parallel orientation, then the degeneracy of $d_{xz}$ and $d_{yz}$ orbitals is removed and the system gains extra stability (vide supra). However, in the case of Fe(II) porphyrin with two axial 1-methylimidazoles, the energy minimum observed is around 80° in order to relieve the steric strain. Thus, potential energy surface (PES) scan results for both Fe(II) and Fe(III) porphyrins show that the energy minimum is observed in one case due to steric reasons, while it is due to electronic reasons for the other case. Thus, the PES scan results further established the fact that the relatively parallel axial orientation is energetically preferred for Fe(III) tetrakis(pentafluorophenyl)-octachloroporphyrin, while a perpendicular orientation is preferred for the Fe(II) complex of the same porphyrin. We have also done the 1D potential energy surface (PES) scan on both Fe(II) and Fe(III) tetranitrooctaethylporphyrins, $Fe^{II}(tn\text{-OEP})(1\text{-MeIm})_2$ and $[Fe^{III}(tn\text{-OEP})(1\text{-MeIm})_2]^+$ (Figures S3


dx.doi.org/10.1021/ic300229u | *Inorg. Chem.* 2012, 51, 11294−11305

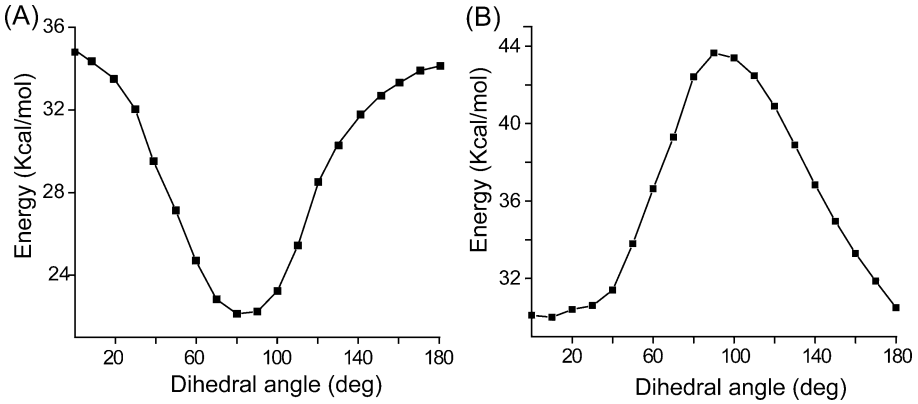


**Figure 6.** Plots showing the relative energy upon changing dihedral angles between two 1-methylimidazoles as axial ligand for (A) $Fe^{II}(TFPPCl_8)(1\text{-}MeIm)_2$ (**2**) and (B) $[Fe^{III}(TFPPCl_8)(1\text{-}MeIm)_2]^+$.

and S4; see the Supporting Information), which show very similar results and are also in close agreement with experiment.

**Cyclic Voltammetric Study.** Cyclic voltammetric experiments for **1** were done at 25 °C under $N_2$ in $CH_2Cl_2$ using 0.1 M tetrabutylammonium perchlorate (TBAP) as the supporting electrolyte. $E_{1/2}$ of the $Fe^{III}/Fe^{II}$ reduction process of **1** is observed at 0.42 V ($\Delta E_p$, 70 mV), a considerably more positive value than those of $Fe^{III}(TPP)Cl$, $Fe^{III}(TFPP)Cl$, and $Fe^{III}(TFPPBr_8)Cl$, which were reported to be −0.29, −0.08, and 0.31 V, respectively.[27d] The ring-centered oxidation of **1** was not observed within the solvent limit (~1.8 V), whereas oxidations of $Fe^{III}(TFPP)Cl$ and $Fe^{III}(TPP)Cl$ occur at 1.50 and 1.30 V, respectively. Thus, complex **1** is much easier to reduce compared to $Fe^{III}(TPP)Cl$ by almost 700 mV, while oxidations are extremely difficult. The addition of 20 fluorines at *meso* phenyl groups and 8 chlorines at *β*-positions in the porphyrin macrocycle serves to both protect the reactive *meso* position from rapid oxidative attack and also stabilize both porphyrin and metal against any oxidative degradation during catalysis. Further, there are no carbon−hydrogen bonds to be oxidatively cleaved, as in TFPP and TPP. Thus, complex **1** can remain catalytically active in a highly oxidizing environment.[27]

Bulk reduction of a dichloromethane solution of **1** at a constant potential of 0.22 V under a nitrogen atmosphere changes the color from brown to green due to the formation of iron(II) complex, which shows a reversible oxidative response at the same potential. Unlike most other iron(II) porphyrins, the electrochemically generated solution of $[Fe^{II}(TFPPCl_8)Cl]^-$ autoxidizes very slowly (days) at 1 atm $O_2$ pressure and 298 K. In contrast, both $Fe^{II}(TFPP)$ and $Fe^{II}(TPP)$ autoxidize rapidly in the presence of oxygen. Moreover, the electronic spectra observed upon bulk oxidation of $[Fe^{II}(TFPPCl_8)Cl]^-$ species at 0.62 V (generated upon bulk reduction of $Fe^{III}(TFPPCl_8)Cl$ (**1**)) exactly overlap with those of $Fe^{III}(TFPPCl_8)Cl$ (Figure 7). Thus, it appears that the iron species remains five-coordinate with chloride in the axial position in the reduced species and there is no loss of chloride ion in the process; otherwise, the autoxidation could show nonisosbestic behavior. Similar results are also observed for $Fe^{III}(tn\text{-}OEP)Cl$ and $Fe^{III}(TFPPBr_8)Cl$.[19a,27d]

Cyclic voltammetry of $Fe^{II}(TFPPCl_8)(L)_2$ was also carried out, and a representative spectrum is shown for $Fe^{II}(TFPPCl_8)(1\text{-}MeIm)_2$ (**2**) in Figure 8A. The $E_{1/2}$ value of the $Fe^{II}/Fe^{III}$ oxidation process is observed at a considerably higher positive value of 0.74 V when 1-methylimidazole is used as the axial ligand. Complexes with imidazole and 4-methylimidazole axial

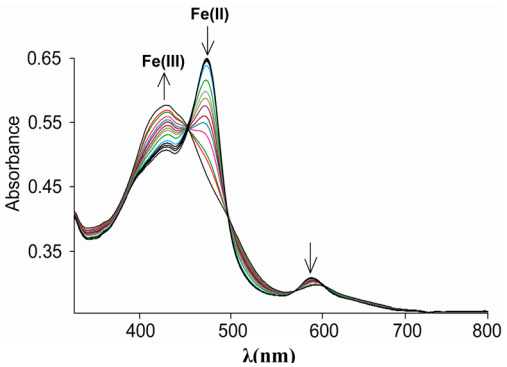


**Figure 7.** Spectral changes upon bulk oxidation of $[Fe^{II}(TFPPCl_8)Cl]^-$ in dichloromethane at 0.62 V, forming $Fe^{III}(TFPPCl_8)Cl$ (**1**). Arrows indicate an increase or decrease of band intensity. Isosbestic points (nm): 437, 585, 602.

ligands also behave similarly. The observed oxidations at such high positive potentials for $Fe^{II}(TFPPCl_8)(L)_2$ readily explain why the complexes are so stable in air. Moreover, metal-centered redox processes are also found to be dependent on the basicity of the axial ligand L in $Fe^{II}(TFPPCl_8)(L)_2$, in which the potential decreases with increasing $pK_a$ values of L.

Bulk oxidation of $Fe^{II}(TFPPCl_8)(1\text{-}MeIm)_2$ (**2**) in dichloromethane at a constant potential of 0.94 V using 0.1 M TBAP as supporting electrolyte under nitrogen changes the color from green to brown, and the progress of the reaction was monitored by UV−visible spectral changes, as shown in Figure 8B. The oxidized product is identified as $[Fe^{III}(TFPPCl_8)(1\text{-}MeIm)_2]ClO_4$, which shows identical UV−vis (at 298 K) and EPR spectra (at 77 K). The species on reduction at 0.54 V regenerates the green solution of **2** again. Similar behavior is also observed when imidazole or 4-methylimidazole is used as the axial ligand. Thus, the axial ligand orientations (parallel and perpendicular) change upon changing the Fe oxidation state of the complexes, as demonstrated in Scheme 4.

On the basis of theoretical and experimental data obtained from model hemes with planar porphyrins which do not possess bulky substituents, there is practically no difference in the preference for parallel or orthogonal orientations of imidazoles for both the Fe(II) and Fe(III) complexes, since they almost have the same energy. For axial ligands to successfully rotate, the ring has to assume a planar conformation in order to allow the ligands to pass over the $Fe-N_p$ bonds and then has to change the direction of its


dx.doi.org/10.1021/ic300229u | *Inorg. Chem.* 2012, 51, 11294−11305

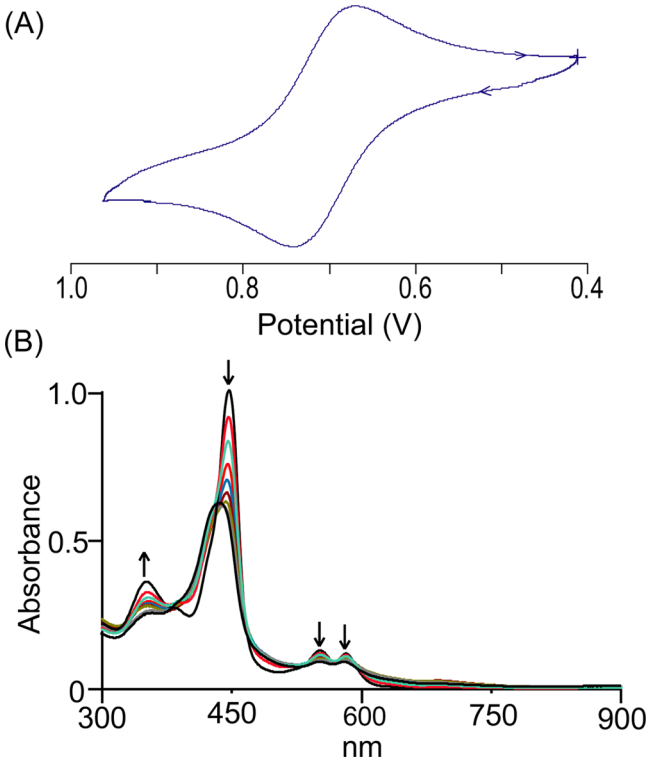


**Figure 8.** (A) Portion of the cyclic voltammogram for $Fe^{II}(TFPPCl_8)(1\text{-MeIm})_2$ (**2**) in $CH_2Cl_2$ (scan rate 100 mV/s) with 0.1 M tetra-*n*-butylammonium perchlorate as supporting electrolyte. The reference electrode was Ag/AgCl. (B) Spectral changes upon oxidation of $Fe^{II}(TFPPCl_8)(1\text{-MeIm})_2$ (**2**) in dichloromethane at a constant potential of 0.94 V under nitrogen at 298 K, forming $[Fe^{III}(TFPPCl_8)(1\text{-MeIm})_2]^+$. Arrows indicate an increase or decrease of band intensity.

distortion by 90°. When the energy difference between parallel and perpendicular forms is very large (due to a highly distorted and dodecasubstituted porphyrin core), the rotation of the axial ligands will be restricted, as observed here.

Even though we have utilized saddle-distorted Fe(III) porphyrinates for the present investigation in order to model the bis-histidine-ligated cytochromes, we are not proposing that the membrane-bound proteins also have highly saddled hemes. Rather, we have used Fe(III) tetrakis(pentafluorophenyl)-octachloroporphyrins because they allow investigating the model heme complexes that are unconstrained by surrounding proteins (in contrast to the membrane-bound heme proteins). Model systems have been very useful in correlating the structures of heme centers with their spectroscopic properties. We have demonstrated here that the iron(II) and iron(III) porphyrinates with two planar and unhindered axial ligands have different orientation preferences in a nonplanar porphyrinic environment. In both $Fe^{II}(TFPPCl_8)(L)_2$ and $[Fe^{III}(TFPPCl_8)(L)_2]^+$, the peripheral substituents are all the same and the substituent effects are thus expected to be similar. However, the conformation and electronic effects should be operative, leading to two different axial orientations.

## CONCLUSIONS

The synthesis, structure, and properties of low-spin bis-imidazole-coordinated Fe(III) and Fe(II) complexes of 5,10,15,20-tetrakis(pentafluorophenyl)-2,3,7,8,12,13,17,18-octachloroporphyrin have been reported here. The X-ray structure of $Fe^{II}(TFPPCl_8)(1\text{-MeIm})_2$ shows near-perpendicular axial ligand orientation (dihedral angles of 80.7°) in a saddle-distorted macrocyclic environment. The experimental result is also supported by a 1D potential energy surface (PES) scan, which shows the lowest energy when the dihedral angle between two axial 1-methylimidazoles is ∼80°. Our observations thus demonstrate conclusively that the relatively perpendicular axial orientation is preferred for unhindered imidazoles as axial ligands in the highly saddle-distorted porphyrin.

Oxidation of $Fe^{II}(TFPPCl_8)(L)_2$ using thianthrenium perchlorate as an oxidizing agent produces $[Fe^{III}(TFPPCl_8)(L)_2]ClO_4$, which was then isolated and characterized spectroscopically. The complex gives rhombic EPR spectra in both the solid state and solution at 77 K and thus represents a rare example of nearly parallel axial ligand orientations for the unhindered imidazoles in a saddle-distorted porphyrin macrocycle. Geometry optimization using DFT converged to the parallel axial alignment with an 8.6° dihedral angle when 1-methylimidazole was used as the axial ligand, which is further supported by a 1D potential surface energy scan. Our observations thus demonstrate that the relatively parallel axial orientation is preferred for unhindered imidazoles as axial ligands in the highly saddle distorted porphyrin.

Electrochemical data obtained from the cyclic voltammetric study of $Fe^{II}(TFPPCl_8)(L)_2$ reveals the one-electron oxidations at very high positive potential, which readily explains why the complex is so stable in air. Moreover, the metal-centered redox process is also found to be dependent on the basicity of the axial ligand L. Bulk oxidation of $Fe^{II}(TFPPCl_8)(L)_2$ in dichloromethane at a constant potential under nitrogen changes the color from green to brown; the oxidized product is then identified as $[Fe^{III}(TFPPCl_8)(L)_2]ClO_4$, which also shows identical EPR spectra at 77 K. The species, upon reduction at a constant potential, regenerates the green solution of $Fe^{II}(TFPPCl_8)(L)_2$ again. Thus, the axial ligand orientations

**Scheme 4**

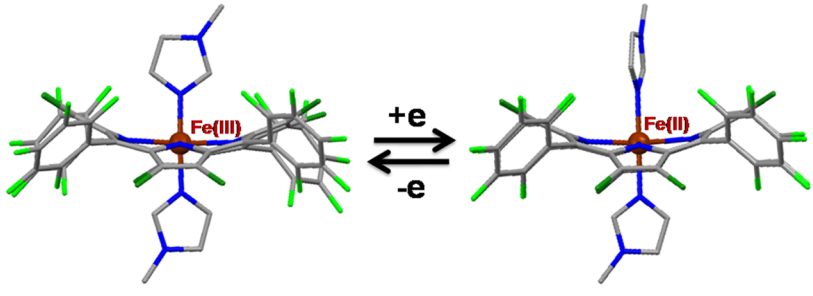



dx.doi.org/10.1021/ic300229u | *Inorg. Chem.* 2012, 51, 11294−11305

switch between parallel and perpendicular just by changing the Fe oxidation state of the complexes.

We have reported here the parallel and perpendicular orientation preferences of two unhindered imidazoles as axial ligands (L) while coordinated to Fe(III) and Fe(II) porphyrins, respectively, in a saddle-distorted porphyrinic environment. Studying the orientation and rotation of axial ligands in model hemes will be extremely useful in understanding the possible effects of various axial ligand orientations that have been observed in analogous heme proteins.

## EXPERIMENTAL SECTION

Reagents and solvents were purchased from commercial sources and purified by standard procedures before use. 5,10,15,20-Tetrakis-(pentafluorophenyl)-2,3,7,8,12,13,17,18-octachloroporphyrin ($H_2TFPPCl_8$) was prepared by using literature methods.[26] Thianthrene perchlorate was prepared using a method reported earlier.[37]

**Preparation of $Fe^{III}(TFPPCl_8)Cl$ (1).** A 80 mg portion of 5,10,15,20-tetrakis(pentafluorophenyl)-2,3,7,8,12,13,17,18-octachloroporphyrin ($H_2TFPPCl_8$; 0.064 mmol) was dissolved in 80 mL of *N*,*N*-dimethylformamide. Excess $FeCl_2$ was added to the solution, and the mixture was refluxed for 2.5 h under nitrogen. After the mixture was cooled to room temperature, 100 mL dichloromethane was added to it, which was then washed well with 0.2 N HCl (2 × 100 mL). The organic layer was separated and dried over anhydrous $Na_2SO_4$. The resulting solution was then evaporated to complete dryness and purified by column chromatography using silica gel. The major fraction eluted with chloroform was collected and vacuum-dried to give a dark brown solid of the complex. Yield: 64 mg, 75%. Anal. Calcd (found): C, 39.59 (39.48); H, 0.00 (0.12); N, 4.19 (4.30). UV−vis (chloroform) [$\lambda_{max}$, nm ($\varepsilon$, $M^{-1}$ $cm^{-1}$)]: 430 (2.53 × $10^5$), 594 (1.22 × $10^3$). EPR data: in solid (77 K), $g_\perp$ = 5.98 and $g_\parallel$ = 2.01; in toluene (77 K), $g_\perp$ = 5.96 and $g_\parallel$ = 2.01. $E_{1/2}$ ($Fe^{2+}/Fe^{3+}$), V ($\Delta E_p$, mV): 0.42 (70).

The complex $Fe^{II}(TFPPCl_8)(L)_2$ was prepared using the general procedure; details are given below for one representative case.

**Preparation of $Fe^{II}(TFPPCl_8)(1\text{-MeIm})_2$ (2).** $Fe^{III}(TFPPCl_8)Cl$ (**1**; 50 mg, 0.037 mmol) was dissolved in 10 mL of dichloromethane. A 30 mg portion of 1-methylimidazole (0.37 mmol) was added to it, and the mixture was stirred for 30 min. The initially brown solution turned red during the progress of the reaction. The resulting solution was then filtered to remove any solid residue and carefully layered with *n*-hexanes. Upon standing for 7−8 days, a dark red crystalline solid was formed, which was collected by filtration, washed well with *n*-hexanes, and dried under vacuum. Yield: 46 mg, 85%. Anal. Calcd (found): C, 42.55 (42.64); H, 0.82 (0.95); N, 7.63 (7.55). UV−vis (chloroform) [$\lambda_{max}$, nm ($\varepsilon$, $M^{-1}$ $cm^{-1}$)]: 380 (2.7 × $10^4$), 446 (1.9 × $10^5$), 552 (6.5 × $10^3$), 582 (6.7 × $10^3$). $^1H$ NMR ($CDCl_3$, 295 K): 1-methylimidazole, 2-*H*, 0.98; 4-*H*, 1.25; 5-*H*, 4.68; 1-$CH_3$, 2.56 ppm. $E_{1/2}$ ($Fe^{2+}/Fe^{3+}$), V ($\Delta E_p$, mV): 0.74 (70).

**$Fe^{II}(TFPPCl_8)(4\text{-MeIm})_2$ (3).** Yield: 41 mg, 75%. Anal. Calcd (found): C, 42.55 (42.47); H, 0.82 (0.99); N, 7.63 (7.71). UV−vis (chloroform) [$\lambda_{max}$, nm ($\varepsilon$, $M^{-1}$ $cm^{-1}$)]: 389 (2.3 × $10^4$), 441 (2.2 × $10^5$), 546 (2 × $10^3$), 576 (4.8 × $10^3$). $^1H$ NMR ($CDCl_3$, 295 K): 4-methylimidazole, 2-*H*, 1.08; 5-*H*, 4.68; 4-$CH_3$, 3.56 ppm. $E_{1/2}$ ($Fe^{2+}/Fe^{3+}$), V ($\Delta E_p$, mV): 0.68 (80)

**$Fe^{II}(TFPPCl_8)(Im)_2$ (4).** Yield: 43 mg, 80%. Anal. Calcd (found): C, 41.70 (41.81); H, 0.56 (0.69); N, 7.78 (7.88). UV−vis (chloroform) [$\lambda_{max}$, nm ($\varepsilon$, $M^{-1}$ $cm^{-1}$)]: 388 (1.9 × $10^4$), 447 (2.8 × $10^5$), 545 (4.5 × $10^3$), 575 (4.7 × $10^3$). $^1H$ NMR ($CDCl_3$, 295 K): 1-methylimidazole, 2-*H*, 1.28; 4-*H*, 1.85; 5-*H*, 4.68 ppm. $E_{1/2}$ ($Fe^{2+}/Fe^{3+}$), V ($\Delta E_p$, mV): 0.78 (70).

The complex $[Fe^{III}(TFPPCl_8)(L)_2]ClO_4$ was prepared using the general procedure; details are given below for one representative case.

**Preparation of $[Fe^{III}(TFPPCl_8)(1\text{-MeIm})_2]ClO_4$ (5).** A 50 mg portion of $Fe^{II}(TFPPCl_8)(1\text{-MeIm})_2$ (**2**; 0.034 mmol) was dissolved in 10 mL of dry dichloromethane. A 13 mg portion (0.042 mmol) of thianthrenium perchlorate was added to the solution, which was then stirred for 2 h under an $N_2$ atmosphere and evaporated to complete dryness. The resultant dark brown solid was dissolved in a minimum volume of dichloromethane and carefully layered with *n*-hexanes which was then kept for $^1/_2$ h at a constant temperature of 5 °C, during which time the crystalline solid of the complex precipitated out. The dark solid was collected by filtration, washed well with *n*-hexanes, and dried under vacuum. Yield: 24 mg, 45%. Anal. Calcd (found): C, 39.84 (39.95); H, 0.77 (0.89); N, 7.15 (7.03). UV−vis (chloroform) [$\lambda_{max}$, nm ($\varepsilon$, $M^{-1}$ $cm^{-1}$)]: 393 sh (2.8 × $10^5$), 428 (3.2 × $10^5$). EPR data: in solid (77 K), $g_1$ = 1.56, $g_2$ = 2.27, $g_3$ = 2.88; in dichloromethane (77 K), $g_1$ = 1.56, $g_2$ = 2.28, $g_3$ = 2.87.

**$[Fe^{III}(TFPPCl_8)(4\text{-MeIm})_2]ClO_4$ (6).** Yield: 27 mg, 52%. Anal. Calcd (found): C, 39.84 (39.73); H, 0.77 (0.91); N, 7.15 (7.24). UV−vis (chloroform) [$\lambda_{max}$, nm ($\varepsilon$, $M^{-1}$ $cm^{-1}$)]: 391 sh (2.6 × $10^5$), 426 (3.1 × $10^5$). EPR data: in solid (77 K), $g_1$ = 1.58, $g_2$ = 2.29, $g_3$ = 2.85; in dichloromethane (77 K), $g_1$ = 1.59, $g_2$ = 2.28, $g_3$ = 2.85.

**$[Fe^{III}(TFPPCl_8)(Im)_2]ClO_4$ (7).** Yield: 22 mg, 42%. Anal. Calcd (found): C, 39.01 (38.90); H, 0.52 (0.64); N, 7.28 (7.19). UV−vis (chloroform) [$\lambda_{max}$, nm ($\varepsilon$, $M^{-1}$ $cm^{-1}$)]: 392 sh (2.4 × $10^5$), 428 (2.8 × $10^5$). EPR data: in solid (77 K), $g_1$ = 1.57, $g_2$ = 2.29, $g_3$ = 2.89; in dichloromethane (77 K), $g_1$ = 1.57, $g_2$ = 2.30, $g_3$ = 2.88.

**Instrumentation.** UV−vis spectra were recorded on a PerkinElmer UV−vis spectrometer. Elemental (C, H, and N) analyses were performed on a CE-440 elemental analyzer. Electron paramagnetic resonance (EPR) spectra were obtained on a Bruker EMX EPR spectrometer. Cyclic voltammetric studies were performed on a BAS Epsilon electrochemical workstation in dichloromethane with 0.1 M tetrabutylammonium perchlorate (TBAP) as supporting electrolyte, Ag/AgCl as the reference electrode, and Pt wire as the the auxiliary electrode. The concentration of the complex was on the order of $10^{-3}$ M. The ferrocene/ferrocenium couple occurs at $E_{1/2}$ = +0.45(65) V versus Ag/AgCl under the same experimental conditions. $^1H$ NMR spectra were recorded on a JEOL 500 MHz instrument. The residual $^1H$ resonances of the solvents were used as a secondary reference.

**X-ray Structure Solution and Refinement.** Crystals were coated with light hydrocarbon oil and mounted in the 100 K dinitrogen stream of a Bruker SMART APEX CCD diffractometer equipped with a CRYO Industries low-temperature apparatus, and intensity data were collected using graphite-monochromated Mo K$\alpha$ radiation ($\lambda$= 0.710 73 Å). The data integration and reduction were processed using SAINT software,[38] and an absorption correction was applied.[39] Structures were solved by the direct method using SHELXS-97 and refined on $F^2$ by full-matrix least-squares techniques using the SHELXL-97[40] program package. Non-hydrogen atoms were refined anisotropically. In the refinement, hydrogens were treated as riding atoms using SHELXL default parameters.

**Computational Details.** DFT calculations have been carried out by employing a B3LYP hybrid functional using the Gaussian 03, revision B.04, package.[36] The method used was Becke's three-parameter hybrid exchange functional,[34] the nonlocal correlation provided by the Lee, Yang, and Parr expression,[35] and Vosko, Wilk, and Nussair 1980 correlation functional (III) for local correction. The basis set was LANL2DZ for the iron atom and 6-31G** for C, N, O, and H. The coordinates are taken directly from the single-crystal X-ray data of **2**. Geometry optimization of $[Fe^{III}(TFPPCl_8)(1\text{-MeIm})_2]^+$ was then performed, keeping the spin state (low spin) constant. For the 1D potential energy surface (PES) scan, the coordinates were taken directly from the X-ray structure and the optimized geometries of Fe(II) and Fe(III) complexes, respectively. For the PES scan on $Fe^{II}(TFPPCl_8)(1\text{-MeIm})_2$ and $[Fe^{III}(TFPPCl_8)(1\text{-MeIm})_2]^+$, one axial ligand was allowed to rotate in steps of 10°, keeping the other axial ligand intact in its position.

## ASSOCIATED CONTENT

### Supporting Information

Selected bond distances and angles of X-ray and geometrically optimized structures of $Fe^{II}(TFPPCl_8)(1\text{-MeIm})_2$ and $[Fe^{III}(TFPPCl_8)(1\text{-MeIm})_2]^+$ (Table S1), a packing diagram of $Fe^{II}(TFPPCl_8)(1\text{-MeIm})_2$ (**2**) (Figure S1), X-band EPR and


dx.doi.org/10.1021/ic300229u | Inorg. Chem. 2012, 51, 11294−11305

simulated spectra of **5** (Figure S2), 1D PES scan for bis(1-methylimidazole) complexes of Fe(III) and Fe(II) tetranitrooctaethylporphyrin (Figures S3 and S4), and a CIF file giving X-ray crystallographic details. This material is available free of charge via the Internet at http://pubs.acs.org.

## AUTHOR INFORMATION


### Corresponding Author

*E-mail: sprath@iitk.ac.in.


### Notes

The authors declare no competing financial interest.

## ACKNOWLEDGMENTS

We are thankful to the CSIR of India and the Department of Science and Technology, Government of India, for financial support. R.P., D.S., S.D., and D.S. thank the CSIR of India for their fellowships.

## DEDICATION

This paper is dedicated to Prof. Parimal K. Bharadwaj on the occasion of his 60th birthday.

## REFERENCES


(1) (a) Mathews, F. A.; Czerwinski, E. W.; Argos, P. In *The Porphyrins*; Dolphin, D., Ed.; Academic Press: New York, 1979; Vol. *7*, p 107. (b) Timkovich, R. In *The Porphyrins*; Dolphin, D., Ed.; Academic Press: New York, 1979; Vol. *12*, p 241.

(2) (a) Brennan, L.; Turner, D. L.; Fareleira, P.; Santos, H. *J. Mol. Biol.* **2001**, *308*, 353. (b) Nørager, S.; Legrand, P.; Pieulle, L.; Hatchikian, C.; Roth, M. *J. Mol. Biol.* **1999**, *290*, 881.

(3) (a) Akutsu, H.; Takayama, Y. *Acc. Chem. Res.* **2007**, *40*, 171. (b) Paquete, C. M.; Louro, R. O. *Dalton Trans.* **2010**, *39*, 4259.

(4) Sun, F.; Huo, X.; Zhai, Y.; Wang, A.; Xu, J.; Su, D.; Bartiam, M.; Rao, Z. *Cell* **2005**, *121*, 1043.

(5) (a) Huang, L.; Cobessi, D.; Tung, E. Y.; Berry, E. A. *J. Mol. Biol.* **2005**, *351*, 573. (b) Palsdottir, H.; Lojero, C. G.; Trumpower, B. L.; Hunte, C. *J. Biol. Chem.* **2003**, *278*, 31303. (c) Gao, X.; Wen, X.; Esser, L.; Quinn, B.; Yu, L.; Yu, C.-A.; Xia, D. *Biochemistry* **2003**, *42*, 9067. (d) Lange, C.; Hunte, C. *Proc. Natl. Acad. Sci. U.S.A.* **2002**, *99*, 2800. (e) Hunte, C.; Koepke, J.; Lange, C.; Rossmanith, T.; Michel, H. *Structure* **2000**, *8*, 669. (f) Iwata, S.; Lee, J. W.; Okada, K.; Lee, J. K.; Iwata, M.; Rasmussen, B.; Link, T. A.; Ramaswamy, S.; Jap, B. K. *Science* **1998**, *281*, 64. (g) Zhang, Z.; Huang, L.; Shulmeister, V. M.; Chi, Y.-I.; Kim, K. K.; Hung, L.-W.; Crofts, A. R.; Berry, E. A.; Kim, S.-H. *Nature* **1998**, *392*, 677. (h) Xia, D.; Yu, C.-A.; Kim, H.; Xia, J.-Z.; Kachurin, A. M.; Zhang, L.; Yu, L.; Deisenhofer, J. *Science* **1997**, *277*, 60.

(6) (a) Cramer, W. A.; Zhang, H.; Yan, J.; Kurisu, G.; Smith, J. L. *Biochemistry* **2004**, *43*, 5921. (b) Smith, J. L.; Zhang, H.; Yan, J.; Kurisu, G.; Cramer, W. A. *Curr. Opin. Struct. Biol.* **2004**, *14*, 432. (c) Stroebel, D.; Choquet, Y.; Popot, J.-L.; Picot, D. *Nature* **2003**, *426*, 413. (d) Durisu, G.; Zhang, H.; Smith, J. L.; Cramer, W. A. *Science* **2003**, *302*, 1009.

(7) (a) Jormakka, M.; Törnroth, S.; Byrne, B.; Iwata, S. *Science* **2002**, *295*, 1863. (b) Einsle, O.; Stach, P.; Messerschmidt, A.; Simon, J.; Kröger, A.; Huber, R.; Kroneck, P. M. H. *J. Biol. Chem.* **2000**, *275*, 39608. (c) Jafferji, A.; Allen, J. W. A.; Ferguson, J. J.; Fülöp, V. *J. Biol. Chem.* **2000**, *275*, 25089. (d) Einsle, O.; Messerschmidt, A.; Stach, P.; Bourenkov, G. P.; Bartunik, H. D.; Huber, R.; Kroneck, P. M. H. *Nature* **1999**, *400*, 476. (e) Michel, H.; Behr, J.; Harrenga, A.; Kannt, A. *Annu. Rev. Biophys. Biomol. Struct.* **1998**, *27*, 329. (f) Crane, B. R.; Siegel, L. M.; Getzoff, E. D. *Science* **1995**, *270*, 59.

(8) (a) Czjzek, M.; Payan, F.; Haser, R. *Biochimie* **1994**, *76*, 546. (b) Pierrot, M.; Haser, R.; Frey, M.; Payan, F.; Astier, J.-P. *J. Biol. Chem.* **1982**, *257*, 14341. (c) Higuchi, Y.; Kusunoki, M.; Matsuura, Y.; Yasuoka, N.; Kakudo, M. *J. Mol. Biol.* **1984**, *172*, 109. (d) Czjzek, M.; Guerlesquin, F.; Bruschi, M.; Haser, R. *Structure* **1996**, *4*, 395. (e) Xia, Z.-X.; Shamala, N.; Bethge, P. H.; Lim, L. W.; Bellamy, H. D.; Xuong, N. H.; Lederer, F.; Mathews, F. S. *Proc. Natl. Acad. Sci. U.S.A.* **1987**, *84*, 2629. (f) Iwata, S.; Ostermeier, C.; Ludwig, B.; Michel, H. *Nature* **1995**, *376*, 660.

(9) (a) Kipke, C. A.; Cusanovich, M. A.; Tollin, G.; Sunde, R. A.; Enemark, J. H. *Biochemistry* **1988**, *27*, 2918. (b) Salerno, J. C. *J. Biol. Chem.* **1984**, *259*, 2331. (c) Tsai, A.-L.; Palmer, G. *Biochim. Biophys. Acta* **1982**, *681*, 484. (d) Tsai, A.-L.; Palmer, G. *Biochim. Biophys. Acta* **1983**, *722*, 349. (e) Berry, M. J.; George, S. J.; Thomson, A. J.; Santos, H.; Turner, D. L. *Biochem. J.* **1990**, *270*, 413. (f) Costa, H. S.; Santos, H.; Turner, D. L.; Xavier, A. V. *Eur. J. Biochem.* **1992**, *208*, 427. (g) Costa, H. S.; Santos, H.; Turner, D. L. *Eur. J. Biochem.* **1993**, *215*, 817.

(10) (a) Protein Data Bank filename 2A06, deposited June, 2005. (b) Howell, N.; Robertson, D. E. *Biochemistry* **1993**, *32*, 11162.

(11) (a) Shelnutt, J. A. In *The Porphyrin Handbook*; Kadish, K. M., Smith, K. M., Guilard, R., Eds.; Academic Press: New York, 2000; Vol. *7*, p 167. (b) Shelnutt, J. A.; Song, X.-Z.; Ma, J.-G.; Jia, S.-L.; Jentzen, W.; Medforth, C. J. *Chem. Soc. Rev.* **1998**, *27*, 31.

(12) Scheidt, W. R. In *The Porphyrin Handbook*; Kadish, K. M., Smith, K. M., Guilard, R., Eds.; Academic Press: San Diego, CA, 2000; Vol. *3*, p 49.

(13) (a) Walker, F. A. *Chem. Rev.* **2004**, *104*, 589. (b) Walker, F. A. *Coord. Chem. Rev.* **1999**, *185−186*, 471.

(14) (a) Furenlid, L. R.; Renner, M. W.; Smith, K. M.; Fajer, J. *J. Am. Chem. Soc.* **1990**, *112*, 1634. (b) Waditschatka, R.; Kratky, C.; Jaun, B.; Heinzer, J.; Eschenmoser, A. *J. Chem. Soc., Chem. Commun.* **1985**, 1604. (c) Geno, M. K.; Halpern, J. *J. Am. Chem. Soc.* **1987**, *109*, 1238. (d) Kratky, C.; Waditschatka, R.; Angst, C.; Johansen, J.; Plaquevent, J. C.; Schreiber, J.; Eschenmoser, A. *Helv. Chim. Acta* **1982**, *68*, 1312.

(15) Anderson, K. K.; Hobbs, J. D.; Luo, L.; Stanley, K. D.; Quirke, J. M. E.; Shelnutt, J. A. *J. Am. Chem. Soc.* **1993**, *115*, 12346.

(16) (a) Berry, E. A; Walker, F. A. *J. Biol. Inorg. Chem.* **2008**, *13*, 481. (b) Rakic, A. A.; Medakovic, V. B.; Zaric, S. D. *J. Inorg. Biochem.* **2006**, *100*, 133. (c) Zaric, S. D.; Popovic, D. M.; Knapp, E. W. *Biochemistry* **2001**, *40*, 7914.

(17) (a) Neya, S.; Suzuki, M.; Hoshino, T.; Ode, H.; Imai, K.; Komatsu, T.; Ikezaki, A.; Nakamura, M.; Furutani, Y.; Kandorib, H. *Biochemistry* **2010**, *49*, 5642. (b) Olea, C., Jr.; Kuriyan, J.; Marletta, M. A. *J. Am. Chem. Soc.* **2010**, *132*, 12794. (c) Olea, C., Jr.; Boon, E. M.; Pellicena, P.; Kuriyan, J.; Marletta, M. A. *ACS Chem. Biol.* **2008**, *3*, 703.

(18) Patra, R.; Chaudhury, A.; Ghosh, S. K.; Rath, S. P. *Inorg. Chem.* **2010**, *49*, 2057.

(19) (a) Patra, R.; Chaudhury, A.; Ghosh, S. K.; Rath, S. P. *Inorg. Chem.* **2008**, *47*, 8324. (b) Ghosh, S. K.; Patra, R.; Rath, S. P. *Inorg. Chem.* **2008**, *47*, 9848. (c) Patra, R.; Rath, S. P. *Inorg. Chem. Commun.* **2009**, 515. (d) Patra, R.; Bhowmik, S.; Ghosh, S. K.; Rath, S. P. *Eur. J. Inorg. Chem.* **2009**, 654. (e) Patra, R.; Bhowmik, S.; Ghosh, S. K.; Rath, S. P. *Dalton Trans.* **2010**, *39*, 5795. (f) Chaudhury, A.; Patra, R.; Rath, S. P. *Indian J. Chem.* **2011**, *50A*, 432.

(20) (a) Medaković, V.; Zarić, S. D. *Inorg. Chim. Acta* **2003**, *349*, 1. (b) Ghosh, A.; Gonzales, E.; Vangberg, T. *J. Phys. Chem. B* **1999**, *103*, 1363.

(21) (a) Shokhirev, N. V.; Shokhireva, T. K.; Polam, J. R.; Watson, C. T.; Raffii, K.; Simons, U.; Walker, F. A. *J. Phys. Chem.* **1997**, *A101*, 2778. (b) Grodzicki, M.; Flint, H.; Winkle, H.; Walker, F. A.; Trautwein, A. X. *J. Phys. Chem.* **1997**, *A101*, 4202. (c) Momot, K. I.; Walker, F. A. *J. Phys. Chem.* **1997**, *A101*, 2787.

(22) (a) Polam, J. R.; Shokhireva, T. K.; Raffi, K.; Simons, U.; Walker, F. A. *Inorg. Chim. Acta* **1997**, *263*, 109. (b) Nakamura, M.; Tajima, K.; Tada, K.; Ishizu, K.; Nakamura, N. *Inorg. Chim. Acta* **1994**, *224*, 113.

(23) Safo, M. K.; Walker, F. A.; Raitsimring, A. M.; Walters, W. P.; Dolata, D. P.; Debrunner, P. G.; Scheidt, W. R. *J. Am. Chem. Soc.* **1994**, *116*, 7760.

(24) (a) Shelnutt, J. A.; Franko, R.; Ma, J. G.; Lu, Y.; Ferreira, G. C. *Biochemistry* **2000**, *39*, 2517. (b) Shelnutt, J. A.; Song, X. Z.; Jenzen,

W.; Jaquinod, L.; Khoury, R. G.; Medforth, C. J.; Jia, S. L.; Ma, J. G.; Smith, K. M. *Inorg. Chem.* **1998**, *37*, 2117.
(25) (a) Moigne, C. L.; Picaud, T.; Boussac, A.; Loock, B.; Momenteau, M.; Desbois, A. *Inorg. Chem.* **2003**, *42*, 6081. (b) Nakamura, M.; Ikezaki, A. *Chem. Lett.* **1995**, 733. (c) Medforth, C. J.; Muzzi, C. M.; Shea, K. M.; Smith, K. M.; Abraham, R. J.; Jia, S.; Shelnutt, J. A. *J. Chem. Soc., Perkin Trans. 2* **1997**, 833.
(26) Chen, H. L.; Ellis, P. E.; Wijesekera, T.; Hagan, T. E.; Groh, S. E.; Lyons, J. E.; Ridge, D. P. *J. Am. Chem. Soc.* **1994**, *116*, 1086.
(27) (a) Grinstaff, M. W.; Hill, M. G.; Labinger, J. A.; Gray, H. B. *Science* **1994**, *264*, 1311. (b) Wijesekera, T.; Matsumoto, A.; Dolphin, D.; Lexa, D. *Angew. Chem.* **1990**, *29*, 1028. (c) Moore, K. T.; Fletcher, J. T.; Therien, M. J. *J. Am. Chem. Soc.* **1999**, *121*, 5196. (d) Grinstaff, M. W.; Hill, M. G.; Birnbaum, E. R.; Schaefer, W. P.; Labinger, J. A.; Gray, H. B. *Inorg. Chem.* **1995**, *34*, 4896.
(28) (a) Hayashi, T.; Nakashima, Y.; Ito, K.; Ikegami, T.; Aritome, I.; Aoyagi, K.; Ando, T.; Hisaeda, Y. *Inorg. Chem.* **2003**, *42*, 7345. (b) Cai, S.; Licoccia, S.; Walker, F. A. *Inorg. Chem.* **2001**, *40*, 5795. (c) Balch, A. L.; Noll, B. C.; Olmstead, M. M.; Phillips, S. L. *Inorg. Chem.* **1996**, *35*, 6495. (d) Del Gaudio, J.; La Mar, G. N. *J. Am. Chem. Soc.* **1978**, *100*, 1112. (e) Del Gaudio, J.; La Mar, G. N. *J. Am. Chem. Soc.* **1976**, *98*, 3014.
(29) (a) Li, J.; Nair, S. M.; Noll, B. C.; Schulz, C. E.; Scheidt, W. R. *Inorg. Chem.* **2008**, *47*, 3841. (b) Silvernail, N. J.; Noll, B. C.; Scheidt, W. R. *Acta Crystallogr., Sect. E* **2005**, *E61*, m1201. (c) Hu, C.; Noll, B. C.; Schulz, C. E.; Scheidt, W. R. *Inorg. Chem.* **2005**, *44*, 4346. (d) Safo, M. K.; Scheidt, W. R.; Gupta, G. P. *Inorg. Chem.* **1990**, *29*, 626. (e) Steffen, W. L.; Chun, H. K.; Hoard, J. L.; Reed, C. A. *Abstracts of Papers*, 175th National Meeting of the American Chemical Society, Anaheim, CA, March 13, 1978; American Chemical Society: Washington, DC, 1978; INOR 15.
(30) (a) Scheidt, W. R.; Noll, B. C. *Acta Crystallogr., Sect. E* **2006**, *E62*, m1892. (b) Kadish, K. M.; Finikova, O. S.; Espinosa, E.; Gros, C. P.; Stefano, G. D.; Cheprakov, A. V.; Beletskaya, I. P.; Guilard, R. *J. Porphyrins Phthalocyanines* **2004**, *8*, 1062.
(31) (a) Ikeue, T.; Ohgo, Y.; Saitoh, T.; Yamaguchi, T.; Nakamura, M. *Inorg. Chem.* **2001**, *40*, 3423. (b) Watson, C. T.; Cai, S.; Shokhirev, N. V.; Walker, F. A. *Inorg. Chem.* **2005**, *44*, 7468. (c) Walker, F. A.; Reis, D.; Balke, V. L. *J. Am. Chem. Soc.* **1984**, *106*, 6888.
(32) (a) Yatsunyk, L. A.; Carducci, M. D.; Walker, F. A. *J. Am. Chem. Soc.* **2003**, *125*, 15986. (b) Teschner, T.; Yatsunyk, L.; Schünemann, V.; Paulsen, H.; Winkler, H.; Hu, C.; Scheidt, W. R.; Walker, F. A.; Trautwein, A. X. *J. Am. Chem. Soc.* **2006**, *128*, 1379. (c) Yatsunyk, L. A.; Dawson, A.; Carducci, M. D.; Nichol, G. S.; Walker, F. A. *Inorg. Chem.* **2006**, *45*, 5417. (d) Hu, C.; Noll, B. C.; Schulz, C. E.; Scheidt, W. R. *Inorg. Chem.* **2006**, *45*, 9721. (e) Ogura, H.; Yatsunyk, L.; Medforth, C. J.; Smith, K. M.; Barkigia, K. M.; Renner, M. W.; Melamed, D.; Walker, F. A. *J. Am. Chem. Soc.* **2001**, *123*, 6564. (f) Silver, J.; Marsh, P. J.; Symons, M. C.; Svistunenko, D. A.; Frampton, C. S.; Fern, G. R. *Inorg. Chem.* **2000**, *39*, 2874. (g) Munro, O. Q.; Serth-Guzzo, J. A.; Turowska-Tyrk, I.; Mohanrao, K.; Shokhireva, T. K.; Walker, F. A.; Debrunner, P. G.; Scheidt, W. R. *J. Am. Chem. Soc.* **1999**, *121*, 11144. (h) Munro, O. Q.; Marques, H. M.; Debrunner, P. G.; Mohanrao, K.; Scheidt, W. R. *J. Am. Chem. Soc.* **1995**, *117*, 935. (i) Safo, M. K.; Gupta, G. P.; Walker, F. A.; Scheidt, W. R. *J. Am. Chem. Soc.* **1991**, *113*, 5497. (j) Higgins, T.; Safo, M. K.; Scheidt, W. R. *Inorg. Chim. Acta* **1990**, *178*, 261. (k) Scheidt, W. R.; Osvath, S. R.; Lee, Y. J. *J. Am. Chem. Soc.* **1987**, *109*, 1958. (l) Scheidt, W. R.; Kirner, J. F.; Hoard, J. L.; Reed, C. A. *J. Am. Chem. Soc.* **1987**, *109*, 1963. (m) Geiger, D. K.; Lee, Y. J.; Scheidt, W. R. *J. Am. Chem. Soc.* **1984**, *106*, 6339. (n) Little, R. G.; Dymock, K. R.; Ibers, J. A. *J. Am. Chem. Soc.* **1975**, *97*, 4532. (o) Collins, D. M.; Countryman, R.; Hoard, J. L. *J. Am. Chem. Soc.* **1972**, *94*, 2066.
(33) Zoppellaro, G.; Harbitz, E.; Kaur, R.; Ensign, A. A.; Bren, K. L.; Andersson, K. K. *J. Am. Chem. Soc.* **2008**, *130*, 15348.
(34) Becke, A. D. *J. Chem. Phys.* **1993**, *98*, 5648.
(35) Lee, C.; Yang, W.; Parr, R. G. *Phys. Rev. B* **1988**, *37*, 785.
(36) Frisch, M. J.; Trucks, G. W.; Schlegel, H. B.; Scuseria, G. E.; Robb, M. A.; Cheeseman, J. R.; Montgomery, J. A., Jr.; Vreven, T.; Kudin, K. N.; Burant, J. C.; Millam, J. M.; Iyengar, S. S.; Tomasi, J.; Barone, V.; Mennucci, B.; Cossi, M.; Scalmani, G.; Rega, N.; Petersson, G. A.; Nakatsuji, H.; Hada, M.; Ehara, M.; Toyota, K.; Fukuda, R.; Hasegawa, J.; Ishida, M.; Nakajima, T.; Honda, Y.; Kitao, O.; Nakai, H.; Klene, M.; Li, X.; Knox, J. E.; Hratchian, H. P.; Cross, J. B.; Bakken, V.; Adamo, C.; Jaramillo, J.; Gomperts, R.; Stratmann, R. E.; Yazyev, O.; Austin, A. J.; Cammi, R.; Pomelli, C.; Ochterski, J. W.; Ayala, P. Y.; Morokuma, K.; Voth, G. A.; Salvador, P.; Dannenberg, J. J.; Zakrzewski, V. G.; Dapprich, S.; Daniels, A. D.; Strain, M. C.; Farkas, O.; Malick, D. K.; Rabuck, A. D.; Raghavachari, K.; Foresman, J. B.; Ortiz, J. V.; Cui, Q.; Baboul, A. G.; Clifford, S.; Cioslowski, J.; Stefanov, B. B.; Liu, G.; Liashenko, A.; Piskorz, P.; Komaromi, I.; Martin, R. L.; Fox, D. J.; Keith, T.; Al-Laham, M. A.; Peng, C. Y.; Nanayakkara, A.; Challacombe, M.; Gill, P. M. W.; Johnson, B.; Chen, W.; Wong, M. W.; Gonzalez, C.; Pople, J. A. *Gaussian 03, revision B.04*; Gaussian, Inc., Pittsburgh, PA, 2003.
(37) Murata, Y.; Shine, H. J. *J. Org. Chem.* **1969**, *34*, 3368.
(38) *SAINT+, 6.02 ed.*; Bruker AXS, Madison, WI, 1999.
(39) Sheldrick, G. M.*SADABS 2.0*; 2000.
(40) Sheldrick, G. M. *Acta Crystallogr.* **2008**, *A64*, 112.